water

MDPI

Article

Activation of Peroxymonosulfate by P-Doped Cow Manure Biochar for Enhancing Degradation of 17β-Estradiol

Wu You [1,2], Gongduan Fan [3,*], Junhou Zhou [3], Ruiyu Lin [1,*], Xingfeng Cao [3], Yiqing Song [3], Jing Luo [4], Jianyong Zou [5], Zhanglin Hong [6], Kai-Qin Xu [3] and Quanda Luo [2]

1 School of Life Sciences, Fujian Agriculture and Forestry University, Fuzhou 350002, China; youwu1986@163.com
2 Fujian Agricultural Ecological Environment and Energy Technology Extension Station, Fuzhou 350001, China; fsnyz@163.com
3 College of Civil Engineering, Fuzhou University, Fuzhou 350116, China; 210527060@fzu.edu.cn (J.Z.); xingfeng_cao@126.com (X.C.); 15159966350@163.com (Y.S.); joexu@fzu.edu.cn (K.-Q.X.)
4 Fujian Jinhuang Environmental Sci-Tech Co., Ltd., Fuzhou 350002, China; irenelj22@163.com
5 Anhui Urban Construction Design Institute Co., Ltd., Hefei 230051, China; medricn@gmail.com
6 China Construction Third Bureau First Engineering Co., Ltd., Wuhan 430040, China; hong198215@126.com
* Correspondence: fgdfz@fzu.edu.cn (G.F.); lrlin2004@163.com (R.L.)

Abstract: Sulfate radical-based advanced oxidation processes exhibit great potential for the degradation of organic pollutants. In this study, P-doped biochar (PBC500) was successfully synthesized by the pyrolysis of H_3PO_4-impregnated cow manure waste and was employed to activate peroxymonosulfate (PMS) for the elimination of 17β-estradiol (E2). The characterization results showed that the surface area, defective structure, and functional groups (C=O and phosphorus-containing groups) of biochar increased after H_3PO_4 modification. PBC500 exhibited high PMS activation activity and excellent E2 degradation capacity; 97.91% of 3 mg/L E2 can be removed within 90 min using 0.2 g/L PBC500 and 1 mM PMS. Based on the quenching experiments and X-ray photoelectron spectroscopy (XPS) analysis, defective structures, C=O, and P-C groups on biochar act as active sites to promote the catalytic oxidation of E2 by generating O_2^- and $^1O_2$. In addition, PBC500 displayed excellent reusability, achieving 65.15% E2 degradation after three reuse cycles. Overall, this study presented a new technique that supports a high efficiency, environmentally friendly, and low cost treatment method for E2 wastewater and simultaneously provided a new option for the resource utilization of livestock waste.

Keywords: P-doped biochar; peroxymonosulfate; 17β-estradiol; advanced oxidation processes

Citation: You, W.; Fan, G.; Zhou, J.; Lin, R.; Cao, X.; Song, Y.; Luo, J.; Zou, J.; Hong, Z.; Xu, K.-Q.; et al. Activation of Peroxymonosulfate by P-Doped Cow Manure Biochar for Enhancing Degradation of 17β-Estradiol. *Water* **2024**, *16*, 1754. https://doi.org/10.3390/w16121754

Academic Editor: Helvi Heinonen-Tanski

Received: 21 May 2024
Revised: 17 June 2024
Accepted: 18 June 2024
Published: 20 June 2024

1. Introduction

Endocrine disrupting chemicals (EDCs) have received widespread attention over recent years because of their severe hazard to human health and ecological safety [1]. The extensive use of estrogen-based medicines and synthetic sex steroids leads to estrogens released in the form of excretions [2]. Moreover, 17β-estradiol (E2) is considered one of the most representative pollutants of EDCs due to its potent endocrine disrupting activity even at extremely low doses [3,4]. E2 can cause serious pathological and toxicological damage to humans and animals, such as an increase in cancer and deformity in humans, reproductive organ modification, and feminization in fishes [5,6]. Accordingly, the elimination of E2 from the environment has emerged as an urgent environmental issue in view of its potential detrimental impacts as a pollutant.

Recently, advanced oxidation processes (AOPs) have been recognized as an effective technology for the degradation of recalcitrant organic pollutants into less or non-toxic chemicals, or even carbon dioxide and water [7,8]. Sulfate radical-based AOPs generated from peroxymonosulfate (PMS) have drawn great attention because sulfate radicals exhibit higher redox potential, longer half-life, and broader pH adaptation range compared

with hydroxyl radical [9,10]. Hitherto, several methods have been applied for activating PMS to generate ROS, which include thermal activation [11], ultrasonic activation [12], UV-irradiation activation [13], and transition metal ion or metal oxide activation [14,15]. However, high energy input and expensive operating costs or potential risk owing to the accidental release of toxic metal ions into the environment limit the application of these activation methods.

Carbonaceous materials such as graphene [16], carbon nanotubes [17], nanodiamonds [18], and biochar [19] are considered to be promising catalysts to activate PMS given their environmental and economic benefits. Biochar has been frequently utilized in the environmental remediation field because of its various positive attributes, including eco-friendliness, simple preparation, and relatively low cost [20,21]. Cow manure contains estrogens, antibiotics, and other toxic compounds because of the extensive use of feedstock additives for disease inhibition and growth promotion in livestock [22]. Although cow manure can be utilized as fertilizer for agriculture, the excretion of cow manure far exceeds the requirements of farmlands, and the harmful substances from livestock manure can enter nearby water bodies via compost added to soil [23,24]. The preparation of biochar from cow manure seems to be a better option because estrogens and antibiotics could be decomposed under pyrolysis, thereby reducing the risk of contamination [25,26].

As for biochar, doping heteroatoms such as P is a proven approach to enhance its catalytic activity [27,28]. The presence of P-doped biochar in the reaction system exhibited superefficient persulfate activation, and the gamma-hexachlorocyclohexane (γ-HCH) degradation efficiency was 10.5-fold greater than that of unmodified biochar, which was related to the remarkable enhancement of the specific surface area, hydrophobicity, and adsorption capacity of the biochar by P-doping treatment [29]. P-doping can also improve catalytic activity by enriching the surface catalytic sites and enhancing the electronic conductivity of biochar [30]. Previous research has confirmed that the phosphoric acid modified biochar is characterized by a large specific surface area, rich pore and defect structure, and abundant surface functional groups [31–33], and these properties possibly lead to high catalytic efficiency. However, the application of P-doped biochar material in the PMS activation process has rarely been reported, and the activation mechanism of peroxymonosulfate by P-doped biochar still needs to be further studied.

In addition, biochar has been demonstrated to be an alternative source of solid fuels [34,35]. The inorganic salts such as phosphate contained in the ash of the combusted phosphoric acid modified biochar might facilitate the activation of PMS. Therefore, the ash of exhausted phosphoric acid modified biochar may be considered as a modifier to improve the catalytic activity of pristine biochar.

Herein, cow manure was selected as raw material to prepare phosphoric acid modified biochar for activating PMS to degrade E2. The influence of H_3PO_4 treatment on intrinsic characteristics and catalytic performances of biochar was explored. Moreover, the XPS analysis and quenching experiments were applied to explain the mechanism of the catalytic process. The reuse of exhausted phosphoric acid modified biochar was also investigated. This work presents an achievable strategy for the recycling of livestock waste and provides a feasible method to eliminate estrogen contaminants.

2. Materials and Methods

2.1. Reagents

The raw cow manure was supplied by a local farm in Fujian province. The gathered air-dried cow manure biomass was crushed into small sizes and then dried at 60 °C until constant weight for subsequent use. In addition, 17β-Estradiol (E2, $C_{18}H_{24}O_2$), hydrochloric acid (HCl), sulfuric acid (H_2SO_4), sodium hydroxide (NaOH), anhydrous methanol (MeOH, CH_3OH) and p-benzoquinone (p-BQ, $C_6H_4O_2$) were obtained from Sinopharm Chemical Reagent Co., Ltd, Shanghai, China. Phosphoric acid (H_3PO_4), potassium monopersulfate triple salt (PMS, $KHSO_5 \cdot 0.5KHSO_4 \cdot 0.5K_2SO_4$), acetonitrile ($C_2H_3N$), ascorbic acid ($C_6H_8O_6$), anhydrous ethanol (EtOH, C_2H_6O), sodium chloride (NaCl), humic acid

(HA, $C_{14}H_{14}N_3NaO_3S$), *tert*-butanol (TBA, $C_4H_{10}O$) and furfuryl alcohol (FFA, $C_5H_6O_2$) were supplied by Aladdin Chemistry Co. Ltd., Shanghai, China. All of the reagents were analytical grade except anhydrous methanol, anhydrous ethanol, *tert*-butanol, furfuryl alcohol and acetonitrile which were guarantee grade.

2.2. Preparation of Biochar

The pretreated cow manure was put into a crucible and pyrolyzed in a muffle furnace at 500 °C for 3 h with a low heating rate (5 °C/min) under oxygen-limited circumstances. The material was ground and passed through a 100-mesh sieve after being cooled to room temperature. Subsequently, it was thoroughly washed with deionized water multiple times, dried to constant weight in an oven set at 60 °C, and kept in dry containers with plastic seal bags. The pristine biochar was denoted as CBC500.

In order to prepare phosphoric acid modified biochar, 10 g of pretreated cow manure was immersed in 100 mL H_3PO_4 (4.25 wt%) at room temperature for 24 h. After that, the dried impregnated material was pyrolyzed at 500, 600, and 700 °C in a muffle furnace, respectively. The pyrolysis conditions and the remaining steps are consistent with the pristine biochar. The phosphoric acid modified biochar synthesized at different pyrolysis temperatures (500, 600, and 700 °C) were marked as PBC500, PBC600, and PBC700, respectively.

As for the reuse of exhausted phosphoric acid modified biochar, the phosphoric acid modified biochar was put into a crucible and pyrolyzed in a muffle furnace at 850 °C for 3 h with a low heating rate (5 °C/min) under the oxygen circumstances to allow complete pyrolysis. The residue of entirely pyrolyzed phosphate modified biochar was collected and mixed at a weight ratio of 1:10 with the pretreated cow manure. Following that, the mixture was dissolved into 40 mL of deionized water and magnetically agitated for 2 h in a water bath at 60 °C. The solid material was then gathered by filtration and dried in an oven to a constant weight. The dried material was pyrolyzed in a muffle furnace under the conditions of 500 and 700 °C. The pyrolysis conditions and the remaining steps are consistent with the pristine biochar. The ash modified biochar prepared at 500 and 700 °C were named ABC500 and ABC700, respectively.

2.3. Experimental Procedure

The E2 solution was prepared as follows: 0.1 g of E2 was dissolved in a small amount of methanol and reconcentrated to 100 mL to obtain an E2 stock solution (1 mg/mL), which was stored in a refrigerator at 5 °C. In the subsequent experiments, different concentrations of E2 solutions were obtained by dilution with ultrapure water.

Batch experiments were conducted in 150 mL conical flasks, which were placed in a thermostatic oscillator at room temperature 25 ± 1 °C. Typically, 10 mg PBC500 and 2 mM PMS were added to a 100 mL solution containing contaminants (E2 = 3 mg/L). At the specific time (0, 5, 10, 20, 30, 45, 60, and 90 min), 0.6 mL reaction solution was taken out and combined with 0.6 mL methanol, then filtered through 0.22 μm nylon membranes and rapidly quenched by ascorbic acid to prevent further reactions. Additionally, effects of reaction conditions, including biochar dosage (0.1, 0.2, 0.3, and 0.5 g/L), PMS dosage (0.1, 0.5, 1.0, 2.0, and 5.0 mM), E2 concentration (1.0, 2.0, 3.0, and 6.0 mg/L), pH (3, 5, 7, 9, and 11), Cl^- (0, 2, 5, and 10 mM), and humic acid (0, 2, 5, and 10 mg/L) were investigated. For quenching experiments, different scavengers such as methanol (MeOH), *tert*-butanol (TBA), p-benzoquinone (p-BQ), and furfuryl alcohol (FFA) were applied to identify the main reactive oxygen species generated in the catalytic system. As regards the reusability tests, the passivated catalysts were collected at the conclusion of each run, repeatedly washed with ethanol and water multiple times, and dried at 60 °C for recycling. All of the experiments were carried out in triplicate, and mean values were presented. The pseudo-first-order kinetic model was used to simulate the E2 degradation of all experiments. Details about the kinetic equation are supplied in Text S1 as Supporting Information.

2.4. Characterization Methods

Characterization methods were used to determine the physicochemical properties of the biochar, and detailed information is given in Text S2.

2.5. Analytical Methods

A detailed description of analytic methods is provided in Text S3.

3. Results and Discussion

3.1. Materials Characterization

As shown in Table S1, the P content of CBC500 and PBC500 were 1004 and 2798 mg/kg, respectively, which indicated that the phosphoric acid impregnation process introduced a significant amount of P.

The morphology changes in biochar before and after phosphoric acid modification were illustrated in the SEM images. It could be clearly observed that CBC500 exhibited a comparatively smooth surface and limited porous structure (Figure 1a). After modification, the surface of PBC500 became much rougher with abundant pore structure (Figure 1b), which could facilitate a larger specific area of PBC500. The phosphoric acid could promote the thermolytic decomposition of the biomass raw material and the generation of phosphate linkages, and the expansion of the biomass structure caused by these phosphate linkages facilitated the production of pores [36].

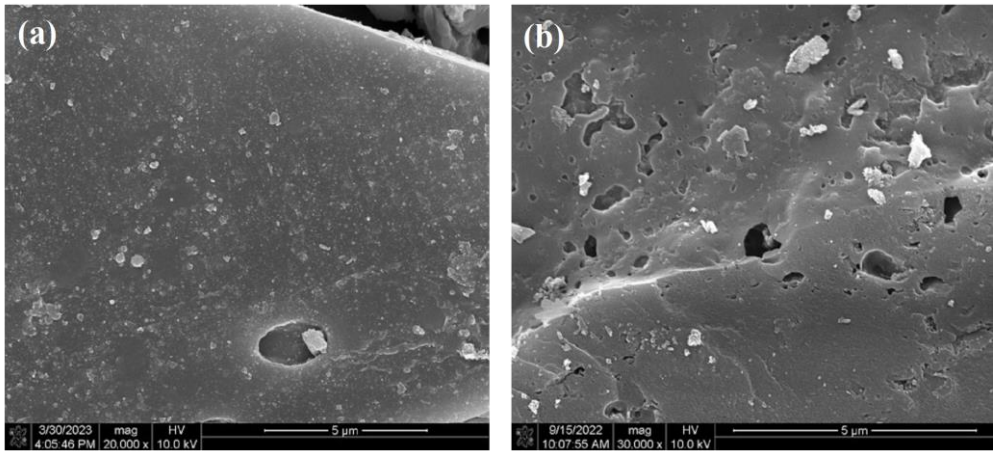

Figure 1. SEM images of the following: (**a**) CBC500; (**b**) PBC500.

The N_2 adsorption/desorption isotherms and pore size distribution of CBC500 and PBC500 are described in Figure 2a. Based on the classification of the International Union of Pure and Applied Chemistry (IUPAC), the isotherms of both CBC500 and PBC500 were determined as type IV curves with H3 hysteresis loops, which was the characteristic of mesopores structure [37]. As shown in Table S2, the BET surface area and total pore volume of PBC500 were 203.77 m^2/g and 0.23 cm^3/g, respectively, which were approximately 16 and 20 times than those of CBC500. This phenomenon demonstrated that phosphoric acid impregnation treatment could effectively improve the pores structure of biochar. These properties of PBC500 would enhance the catalytic performance by promoting the adsorption of target contaminants and PMS molecules in solution on the catalyst surface and speeding electron transfer capability [38].

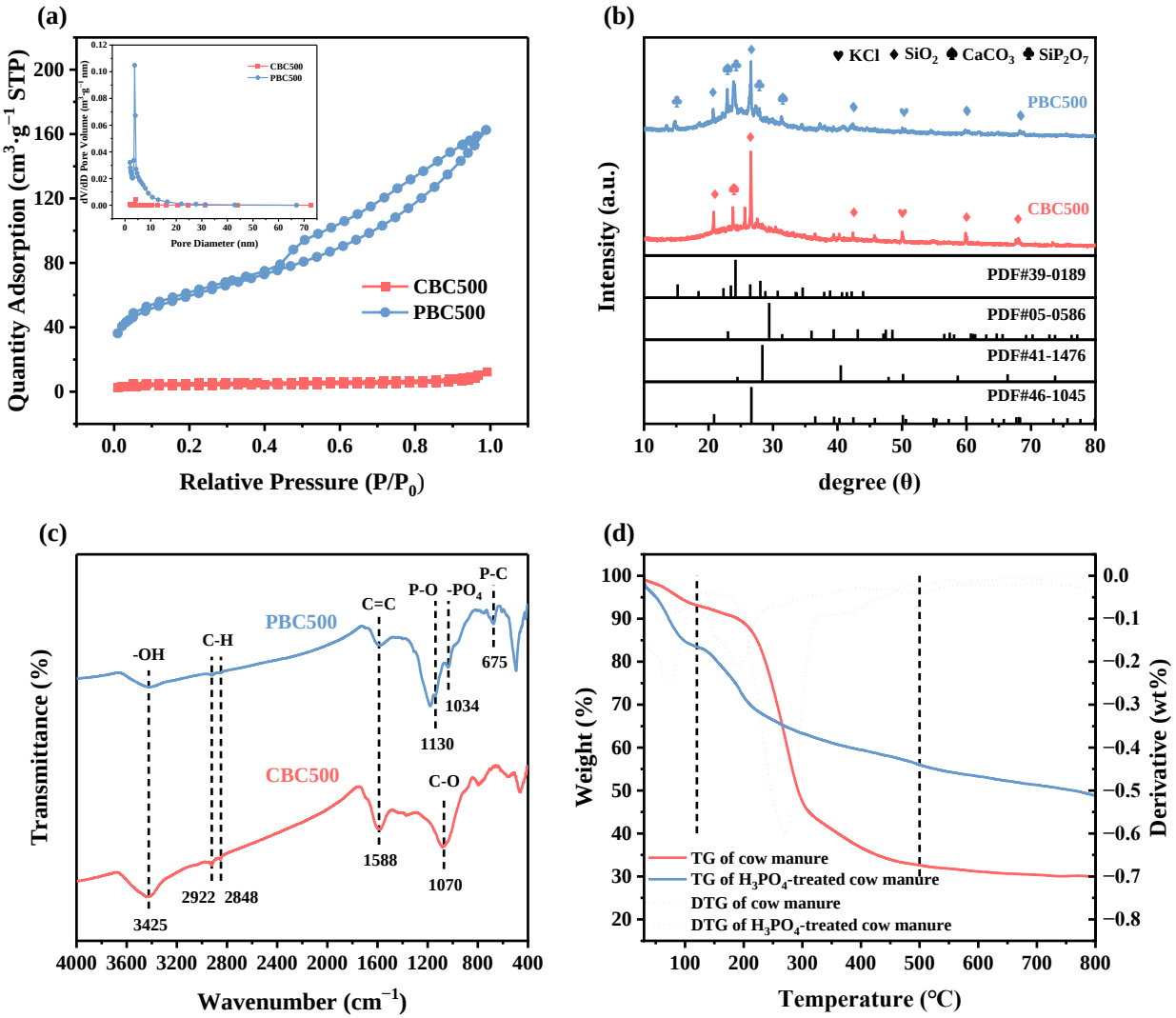

Figure 2. (**a**) N_2 adsorption/desorption isotherms (Inset: Pore size distribution) of CBC500 and PBC500. (**b**) XRD patterns of CBC500 and PBC500. (**c**) FTIR spectra of CBC500 and PBC500. (**d**) TG and DTG curves of untreated and H_3PO_4-treated cow manure.

The crystalline structures of unmodified and modified biochar were analyzed by XRD. As depicted in Figure 2b, quartz (SiO_2, PDF#46-1045), calcite ($CaCO_3$, PDF#05-0586), and sylvite (KCl, PDF#41-1476) were the major mineral crystals on biochar, which may be obscure the presentation of functional groups and crystalline structure of carbon fractions [39]. Moreover, it can be clearly seen that the distinct silicon phosphate (SiP_2O_7, PDF#39-0189) diffraction peaks appeared on the PBC, which was due to the reaction of phosphoric acid with the silicon element in the raw material during the pyrolysis process. After phosphoric acid modification, the intensity of these peaks decreased. There were two distinct broad peaks can be observed at 2θ of around 25° and 40°, which related to the (002) and (100) crystal planes of graphite carbon, and that could reflect the degree of graphitization of biochar [40]. After modification, the noticeably higher intensity of the characteristic peak at around 25° was an implication of the higher graphitization degree of PBC500. Previous studies indicated that the graphite structure of biochar can be used as a bridge for direct electron transfer to persulfate, and the greater graphitization of biochar could lead to better electrical conductivity [41,42].

The main surface functional groups of CBC500 and PBC500 were verified through the FTIR analysis. As illustrated in Figure 2c, the common peaks at around 3425, 2922–2848, 1700, and 1588 cm^{-1} were on CBC500 and PBC500 were associated with -OH stretching, C-H

stretching, C=O stretching and the vibration of C=C, respectively [43–45]. This indicated that CBC500 and PBC500 had similar functional groups. The peak corresponding to C-O stretching shifted from 1070 to 1180 cm^{-1} after modification, probably due to the reaction of phosphoric acid with it. Furthermore, the new peaks at around 1130, 1034, and 675 cm^{-1} that appeared in PBC500 could be attributed to the stretching vibration of P-O, -PO_4, and P-C, respectively [46,47]. This suggested that phosphoric acid modification treatment could successfully load phosphorus onto biochar and form phosphorus-containing phosphate functional groups on its surface.

The surface chemical composition of CBC500 and PBC500 was further detected by XPS spectra. The XPS survey spectra (Figure 3f) revealed that C 1s and O 1s were common peaks of CBC500 and PBC500. In addition, the new peak corresponding to P 2p was obviously detected in the XPS spectra of PBC500, which demonstrated that P was successfully carried on the surface of PBC500. There were four characteristic peaks located at 284.40, 285.00, 286.00, and 288.50 eV could be observed in the XPS spectra of C 1s (Figure 3a,b), which was ascribed to the primary C-C peak from aromatic C-C/C-H bonds, defective carbon structures (C-C high defects), C-O bonds and C=O bonds, respectively [43,48]. After modification, there was a significant reduction in the content of C-C and C-O bonds, while the proportion of C=O and defective carbon structures increased. The O 1s XPS spectra (Figure 3c,d) can be separated into three peaks that represent the C=O, -OH, and C-O bonds [49]. As for the P 2p spectra of PBC500 (Figure 3e), the characteristic peak at 133.27 eV could be associated with the formation of P-C, and the peak situated at around 134.75 eV was attributed to the P-O [50], which also proved that the carbon framework of biochar containing some P atoms. In conclusion, the phosphoric acid impregnation treatment altered the elemental and chemical composition of biochar and made it possess more diverse surface functional groups.

Figure 2d presents the thermogravimetric (TG) and derivative thermogravimetric (DTG) curves of the untreated and H_3PO_4-treated cow manure. The thermal weight loss ratio could be applied to reflect the thermal stability of raw materials. The thermal weight loss ratios of the untreated and phosphoric acid-treated cow manure were 29.90% and 48.88%, respectively, which indicated that phosphoric acid impregnation treatment could significantly enhance the thermal stability of cow manure. There were three distinct stages involved in the pyrolysis processes of all raw materials. The first stage was attributed to the evaporation of moisture and light volatiles and that occurred in the range from 30 to 120 °C; the second stage of weight loss took place in the period from 120 to 500 °C and was mainly owing to the rapid devolatilization and degradation of hemicellulose and cellulose, and the weight loss above 500 °C of the last stage represented the decomposition of lignin and other organic matter with stronger chemical bonds [51]. The second stage of weight loss of phosphoric acid-impregnated cow manure was much lower than that of untreated cow manure (Figure 2d). This phenomenon was probably due to some bonds of hemicellulose, cellulose, and lignin being broken by phosphoric acid, and less energy was required for the pyrolysis of the raw materials [52]. Moreover, the lower weight loss ratio of H_3PO_4-impregnated cow manure may be attributed to the fact that the phosphate chains generated during the process of chain and bond breakage can result in the formation of organic polymers [53].

3.2. E2 Degradation in Different Systems

The E2 adsorption performance of phosphoric acid modified biochar under various pyrolysis temperatures is shown in Figure S1a. The adsorption efficiencies of PBC500, PBC600, and PBC700 on E2 were 46.45%, 40.96%, and 31.97% within 90 min, respectively, among which PBC500 presented the highest adsorption effect. Figure S1b illustrates the performance of phosphoric acid modified biochar obtained under various pyrolysis temperatures on the activation of PMS. It could be observed that PMS showed very low reactivity toward E2, and the incorporation of phosphoric acid modified biochar as a catalyst can lead to a dramatically higher degradation efficiency of E2. The E2 removal

efficiency gradually decreased when the temperature of pyrolysis rose from 500 to 700 °C, which might be because the functional groups of biochar were reduced at higher pyrolysis temperature [54]. As a result, the phosphoric acid modified biochar and the unmodified biochar pyrolyzed at 500 °C were used for subsequent experiments and analyses.

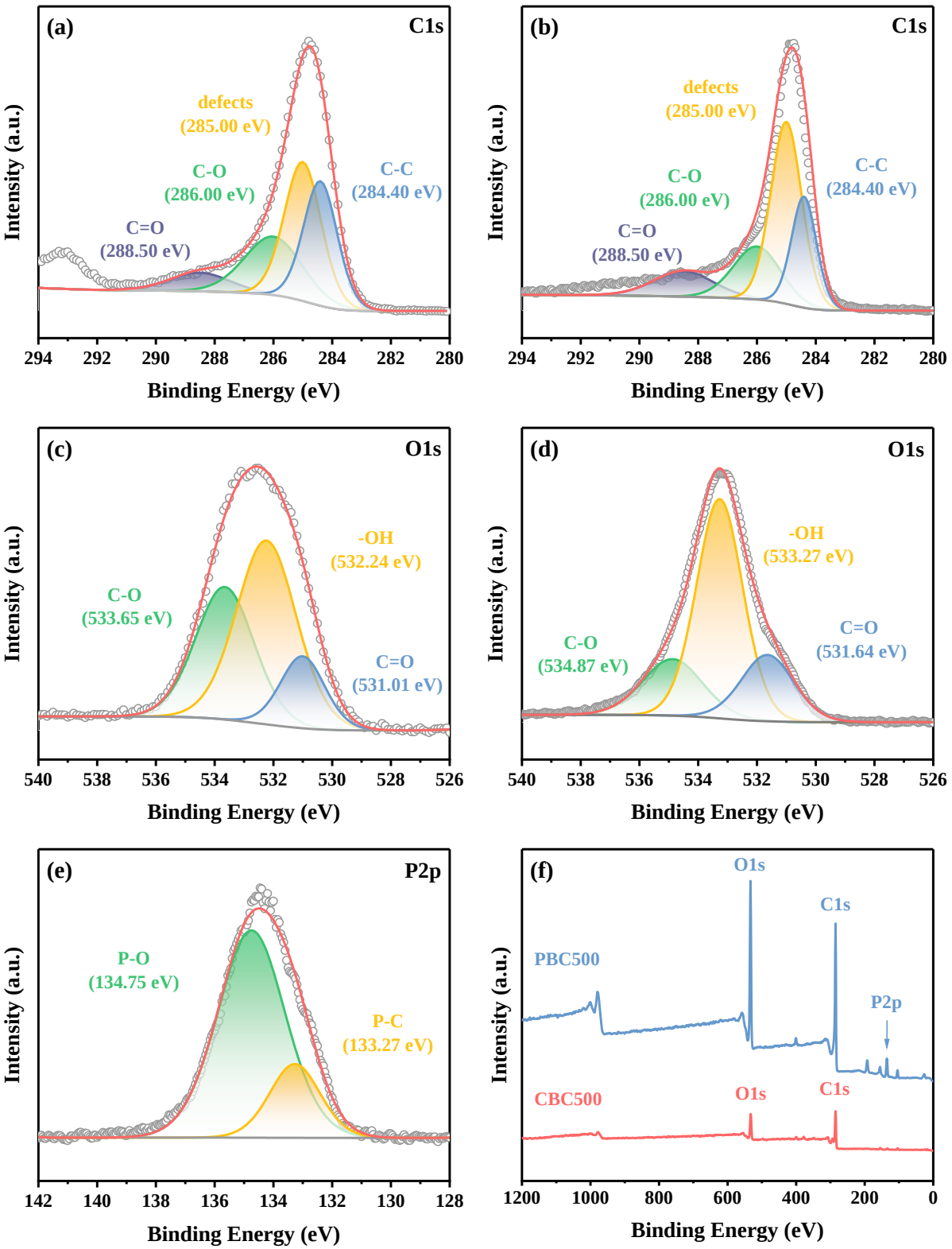

Figure 3. C 1s spectra of (**a**) CBC500 and (**b**) PBC500; O 1s spectra of (**c**) CBC500 and (**d**) PBC500; (**e**) P 2p spectra of PBC500 and (**f**) XPS survey spectra of PBC500 and CBC500.

The impregnation concentration of phosphoric acid determined the pore structure and active sites of the biochar, which in turn affected its activation performance. Figure S2 compares the adsorption and catalytic performance of modified biochar prepared under 2.25 wt%, 4.25 wt%, and 8.50 wt% phosphoric acid impregnation. The results showed that impregnation with phosphoric acid at a concentration of 4.25 wt% was the optimal pretreatment condition. An excessive concentration of phosphoric acid may lead to the destruction of the biomass structure, which caused the collapse of the skeleton of biochar during pyrolysis and made it difficult to form well-developed pores. At the same time, a low concentration of phosphoric acid impregnation may result in insufficient adsorption sites.

Figure 4a illustrates the removal of E2 in a variety of reaction systems. For the unmodified and phosphoric acid modified biochar in the absence of PMS, the E2 removal efficiencies were 17.15% and 44.97% within 90 min, respectively. The superior adsorption performance of PBC500 could be accounted for by its improved physicochemical properties. The removal of E2 by PMS without catalyst activation was only 9.89% within 90 min, which was almost negligible. On the contrary, the removal efficiency of E2 could be improved by biochar activated PMS. It was apparent that PBC500 showed a greater activation capacity for PMS compared to CBC500. It was capable of removing 92.57% E2 within 90 min through the PBC500/PMS system, indicating that PBC500 can effectively activate PMS for E2 degradation. After modification, the large surface area, the greater defect degree, and the higher functional group content of PBC500 might lead to significantly enhanced activation within the PBC500/PMS system, thus facilitating the degradation of E2 [55]. Additionally, the experimental data of E2 removal in various reaction systems were fitted by the pseudo-first-order kinetic model (Figure 4b). The reaction rate constant k_{obs} of E2 degradation in PBC500/PMS system was 0.02502 min^{-1}, which was much greater than that of PMS (k_{obs} = 0.00099 min^{-1}), CBC500 (k_{obs} = 0.00189 min^{-1}), PBC500 (k_{obs} = 0.00648 min^{-1}) and CBC500/PMS (k_{obs} = 0.00757 min^{-1}). This phenomenon also indicated that E2 was removed faster in the PBC500/PMS system.

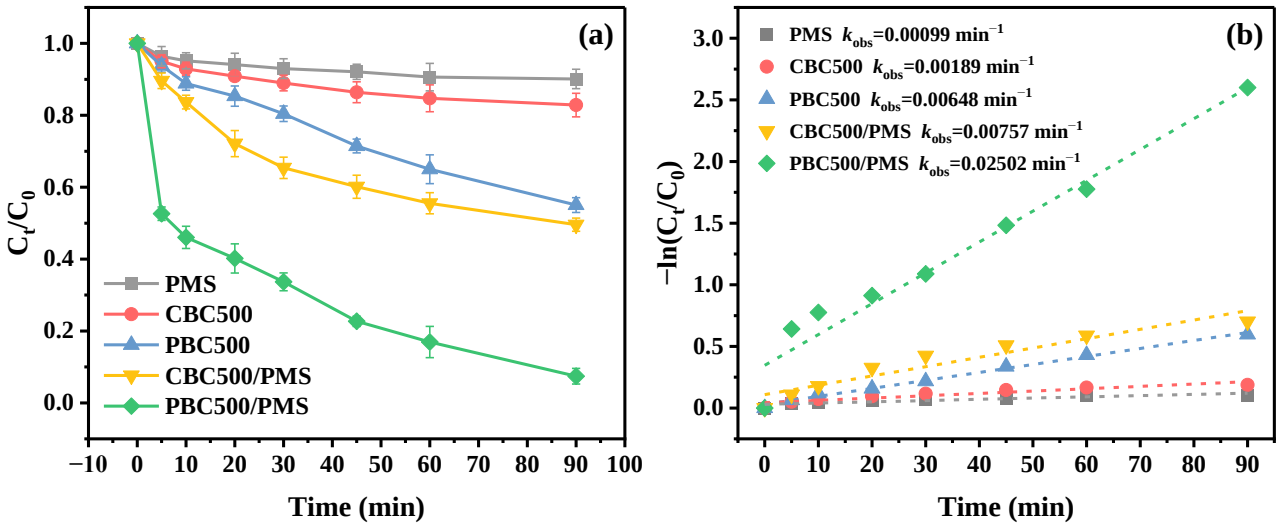

Figure 4. (**a**) Removal of E2 in different systems; (**b**) Kinetic fitting curves (experiment conditions: [E2] = 3 mg/L, [PMS] = 2.0 mM, and [biochar] = 0.1 g/L).

During the reaction, adsorption and oxidation together facilitate the removal of E2 from the aqueous solution. To investigate the relation between adsorption and oxidation, PMS was added after the adsorption of PBC500 reached equilibrium; that is, the adsorption phase and oxidation phase were separate, and the results are shown in Figure S3. It was noteworthy that the degradation efficiency of E2 in a mixed system is lower than that in an individual system, which may be due to the adsorption of E2 on the surface of the catalyst, which was more favorable for its catalytic degradation [56]. Moreover, the concentration

of E2 first increased in different degrees when PS was added to the solutions. This might be because PMS was more readily adsorbed on biochar surface than E2, resulting in the desorption of E2 from the limited adsorption sites.

3.3. Effects of Reaction Conditions on E2 Degradation by PBC500/PMS System

3.3.1. Effect of Catalyst Dosage

As presented in Figure 5a, the removal efficiencies of E2 were 92.26%, 99.21%, 99.30%, and 99.23% within 90 min at the catalyst dosages of 0.1, 0.2, 0.3, and 0.5 g/L, respectively. The corresponding k_{obs} value increased from 0.02718 to 0.07031 min^{-1} when the PBC500 dosage was raised from 0.1 to 0.5 g/L (Figure S5a). The higher dosage of the catalyst could offer a larger surface area and more reaction sites for pollutant adsorption and PMS activation, which might be responsible for the improvement of E2 removal efficiency [57]. However, excessive dosage of the catalyst had limited improvement in E2 removal efficiency and may also result in the lower utilization efficiency of active sites on PBC500. In consideration of the excellent E2 degradation efficiency of E2 and cheap cost of application, the PBC500 dosage of 0.2 g/L was utilized in the subsequent experiments.

3.3.2. Effect of PMS Concentration

Figure 5b depicts the effect of different PMS concentrations on E2 degradation in the PBC500/PMS system. When the PMS concentration raised from 0.1 to 1.0 mM, the degradation efficiency of E2 significantly increased from 90.43% to 98.11% within 90 min, and the corresponding reaction rate constant k_{obs} also posed a rising trend from 0.02670 to 0.04289 min^{-1} (Figure S5b). The higher concentration of PMS exhibited an advantageous impact on E2 degradation, which can be explained by the fact that PMS was able to fully utilize the active sites on PBC500 to produce more reactive oxygen species during the activation process. However, there was no discernible variation in E2 degradation efficiency at 90 min when the PMS concentrations were 1.0, 2.0, and 5.0 mM. This phenomenon may be caused by the limited active sites on PBC500, which were unable to accommodate the excessive PMS, and too much PMS would lead to a self-quenching effect [58].

3.3.3. Effect of E2 Concentration

The effect of the initial E2 concentration on the degradation reaction can be seen from Figure 5c. It was apparent that the increase in E2 concentration adversely affected the E2 degradation reaction. To be specific, it was able to achieve an almost complete removal of E2 within 90 min when the E2 concentration was raised from 1.0 mg/L to 3.0 mg/L, but the removal efficiency was only 76.54% within 90 min when the E2 concentration increased to 6.0 mg/L. In addition, the k_{obs} value also showed a tendency toward decline as a higher E2 concentration (Figure S5c). The probable explanation was that the active sites on PBC500 were covered by excessive E2, which prevented its contact with PMS, leading to the reduction of the reactive oxygen species.

3.3.4. Effect of Solution pH

The initial solution pH affected the degradation performance of the contaminant by determining the catalyst charge, contaminant forms, and PMS species [59]. As illustrated in Figure 5d, the degradation efficiency of E2 reduced from 98.91% to 89.65% within 90 min as the pH value increased from 3 to 11. PMS mainly existed in the form of HSO_5^- as the pH value was below 9.4, and SO_5^{2-} as the pH value was above 9.4 [60]. As observed from Figure S4, the zeta potential of the PBC500 surface was negatively charged in the pH range from 3 to 11, and it decreased with the rise of the solution's pH value. As a result, the greater electrostatic repulsion between PBC500 and PMS was caused by the higher solution pH value, which weakened the activation of PBC500 for PMS. It was also reported that PMS would decompose under the condition of high OH^- concentration (Equation (1)) [61], which might also contribute to the inefficient degradation of E2 in a high pH environment. It was noticeable that the E2 degradation showed a sharp decline when the solution pH

value was raised to 11, which was probably ascribed to the oxidation performance of SO_5^{2-} and was lower than that of HSO_5^- [62]. In addition, E2 (pKa = 10.4 [63]) was negatively charged when pH > pKa (pH = 11), and the repulsive electrostatic interaction between PBC500 and E2 might also be responsible for the reduced E2 removal efficiency at pH 11.

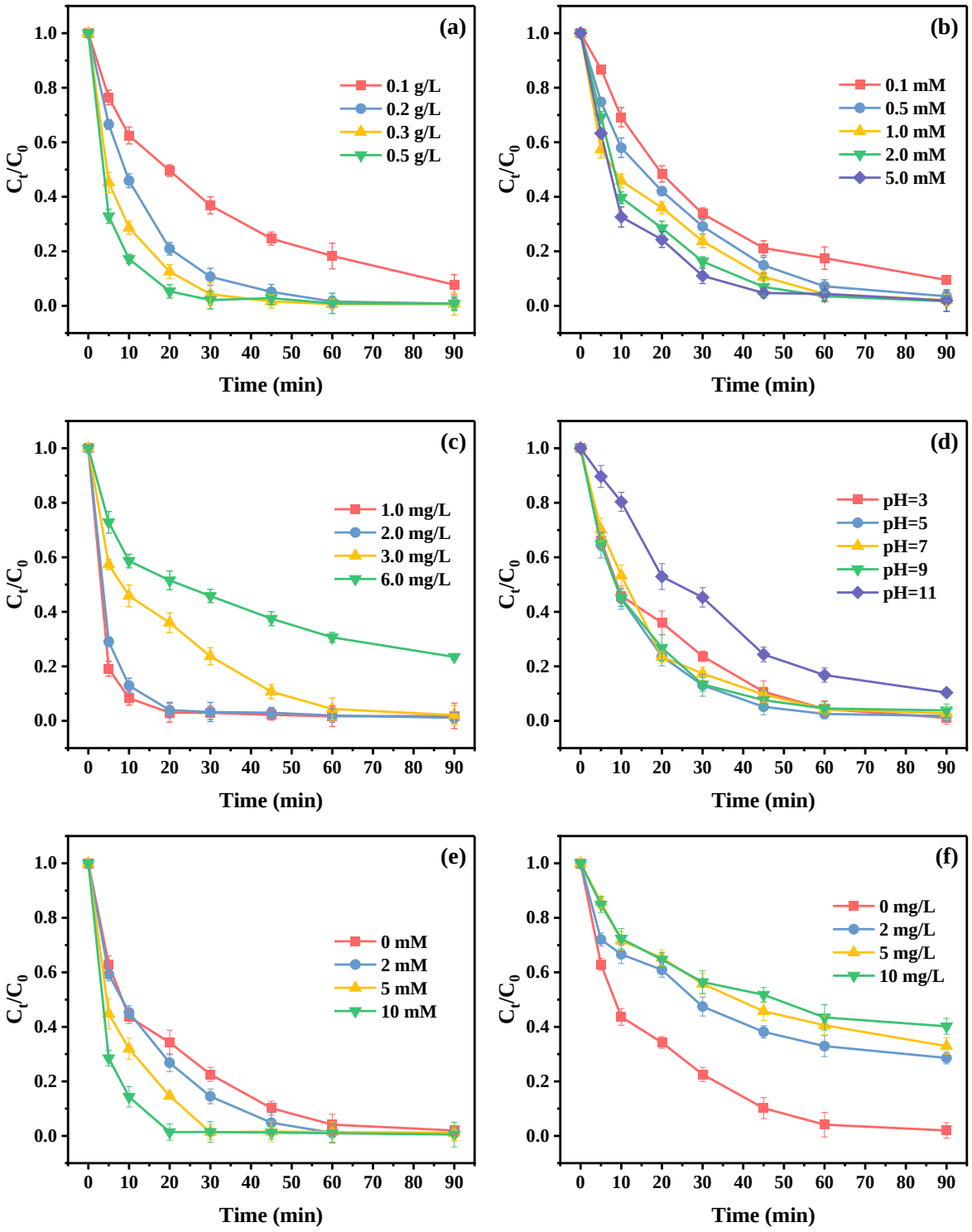

Figure 5. Effects of (**a**) PBC500 dosage ([E2] = 3 mg/L, [PMS] = 2 mM); (**b**) PMS concentration ([E2] = 3 mg/L, [PBC500] = 0.2 g/L); (**c**) E2 concentration ([PMS] = 1 mM, [PBC500] = 0.2 g/L); (**d**) pH, (**e**) Cl^-; (**f**) HA ([E2] = 3 mg/L, [PMS] = 1 mM, [PBC500] = 0.2 g/L) on the degradation of E2 in PBC500/PMS system.

$$HSO_5^- + 2OH^- \rightarrow H_2O + 2SO_4^{2-} + O_2 \quad (1)$$

3.3.5. Effect of Inorganic Anions

Inorganic anions are commonly presented in natural water bodies, which can potentially impact the target contaminants' removal efficiency by occupying active sites on biochar or reacting with some reactive oxygen species. Therefore, Cl^- was selected as the representative inorganic anion to determine its influence on E2 removal in the PBC500/PMS system. As depicted in Figure 5e, the addition of Cl^- obviously exerted a positive role in the removal of E2. When the concentrations of Cl^- were 0, 2, 5, and 10 mM, the k_{obs} values of E2 degradation were 0.044371, 0.05569, 0.07612, and 0.09875 min^{-1}, respectively (Figure S5e). This phenomenon might be due to the excessive Cl^- can be easily oxidized by PMS to generate $HOCl/Cl_2$ with stronger oxidation capacity (Equations (2) and (3)), which can facilitate the removal of E2 [64].

$$Cl^- + HSO_5^- \rightarrow SO_4^{2-} + HClO \quad (2)$$

$$2Cl^- + H^+ + HSO_5^- \rightarrow SO_4^{2-} + Cl_2 + H_2O \quad (3)$$

3.3.6. Effect of HA

As representative organic matter, humic acid (HA) was extensively distributed in natural water bodies. Therefore, the removal of E2 in the PBC500/PMS system under the conditions of different HA concentrations was analyzed. As demonstrated in Figure 5f, it was clear that the E2 removal was dramatically inhibited with the increasing concentration of HA. When the HA concentration was adjusted to 0, 2, 5, and 10 mg/L, the E2 removal efficiencies with 90 min were 98.01%, 71.42%, 67.06%, and 59.78%, respectively. Meanwhile, the corresponding k_{obs} were 0.04371, 0.01319, 0.01193, and 0.00968 min^{-1}, respectively (Figure S5f). The decreased E2 removal efficiency may be associated with the occupation of active sites on PBC500 by excessive HA, which caused the inferior activation performance of PBC500 toward PMS and reduced the generation of ROS [65]. The introduction of substantial amounts of oxygen-containing functional groups on the surface of PBC500 resulted in a notable increase in the density of polar groups, which in turn led to a more hydrophilic surface of PBC500 [66]. As a result, the hydrophilic HA was easier to adsorb on the surface of PBC500, which made the PBC500/PMS system less resistant to HA. In addition, previous research has confirmed that HA can be used as a radical scavenger reacting with the sulfate and hydroxyl radicals [67], and this also led to an enhanced inhibition of E2 degradation.

3.4. Mechanism of E2 Degradation by PBC500/PMS System

3.4.1. Identification of Reactive Oxygen Species

In order to identify the contribution of the ROS during the E2 degradation process, methanol (MeOH), *tert*-butanol (TBA), p-benzoquinone (p-BQ), and furfuryl alcohol (FFA) were selected as scavengers to carry out quenching experiments. MeOH could be used as the efficient scavenger for both SO_4^- (k = 1.6–7.7 × 10^7 $M^{-1}s^{-1}$) and ·OH (k = 1.2–2.8 × 10^9 $M^{-1}s^{-1}$), while TBA was proved to possess excellent quenching efficiency only for ·OH (k = 3.8-7.6 × 10^7 $M^{-1}s^{-1}$) [56]. FFA and p-BQ can be used to quench $^1O_2$ (k = 1.2 × 10^8 $M^{-1}s^{-1}$) and O_2^- (k = 0.9–1.0 × 10^9 $M^{-1}s^{-1}$), respectively [68,69]. The following can be obtained from Figure 6a: the removal efficiencies of E2 declined from 97.91% to 93.73% and 91.32% after the inclusion of MeOH and TBA to the reaction system, respectively, which implicated the presence of SO_4^- and·OH in the E2 degradation process. However, the inhibitory effects on E2 removal caused by MeOH and TBA were negligible, revealing that SO_4^- and ·OH were not the predominant ROS. The E2 removal efficiencies were drastically inhibited with the existence of p-BQ and FFA, which sharply decreased from 97.91% to 38.48% and 34.22%, respectively. This phenomenon indicated that O_2^- and

$^1O_2$ both participated in the E2 elimination process and played the dominant roles. Considering the aforementioned findings, it could be derived that $SO_4^{\cdot-}$, ·OH, $O_2^{\cdot-}$, and $^1O_2$ were all implicated in the E2 degradation process and achieved excellent E2 degradation through radical and non-radical pathways.

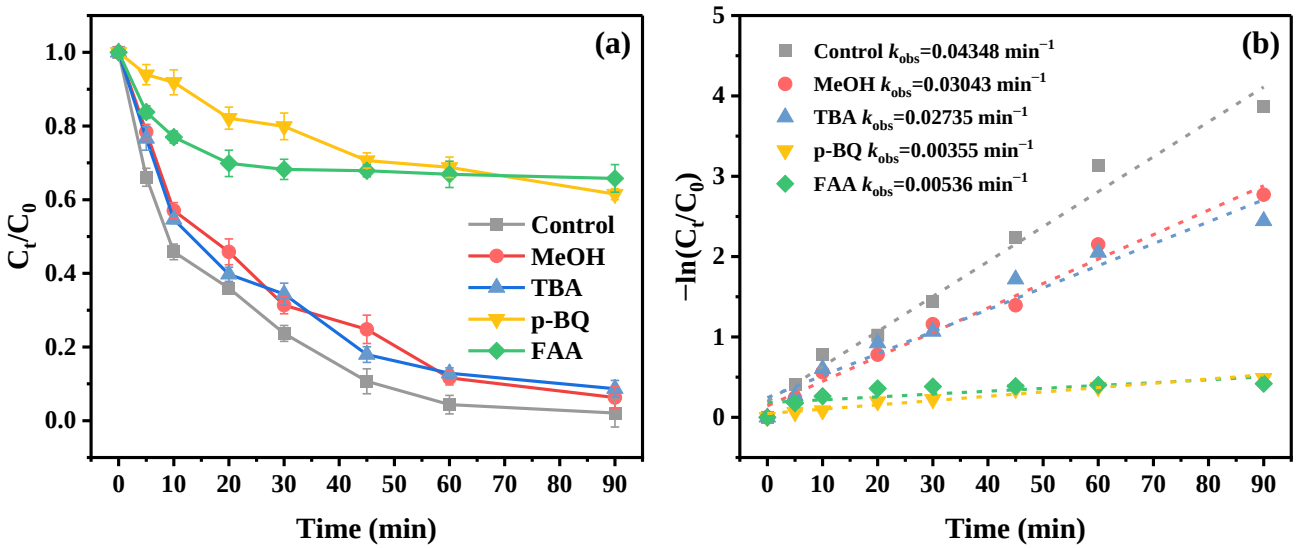

Figure 6. (**a**) The effect of quenchers on E2 degradation. (**b**) Kinetic fitting curves (experiment conditions: [E2] = 3 mg/L, [PMS] = 1.0 mM, and [PBC500] = 0.2 g/L).

3.4.2. Activation Mechanism

The XPS spectra of PBC500 after the E2 degradation reaction were analyzed to further elucidate the activation mechanism of PMS. As reflected in C 1s spectra of PBC500 after the catalytic reaction of E2 (Figure S6a), the proportion of primary C-C increased from 24.74% to 27.48% and C-O increased from 22.32% to 28.13%, while the defective carbon structures significantly dropped from 39.29% to 34.22% and C=O also decreased from 13.65% to 10.17%, demonstrating that C=O and defective structures served as effective active sites participated in the degradation reaction. The transformation of oxygen-containing functional groups on PBC500 after the reaction could be observed in the O 1s XPS spectra (Figure S6b). After the E2 degradation reaction, the higher value of O 1s binding energy indicated that a certain number of electrons were transferred from O to PMS during the activation process [70,71]. In addition, the proportion of C=O reduced from 20.47% to 17.03%, which further demonstrated that C=O exerted a beneficial role during the E2 degradation. In the P 2p spectra (Figure S6c), part of the P-C was converted to the P-O after use, implying that P-C on PBC500 might participate in the catalytic reaction process. According to the previous study, the metaphosphoric acid linked to oxygen atoms and metaphosphoric acid linked in a bridging manner on the surface of biochar both performed an essential role in activating PMS [72]. Therefore, it can be deduced that some specific functional groups and defective structures on PBC500 could be employed as active sites to encourage PMS activation and ROS formation.

In light of the aforementioned results and analyses, the possible mechanism of PBC500 activating PMS to degrade E2 was hypothesized (Figure 7). Firstly, parts of E2 and PMS were adsorbed on the surface of PBC500 because of their characteristics of large specific surface area and abundant pore structure. Subsequently, a variety of reactive oxygen species were produced through the interactions between PMS and effective active sites, such as the defective carbon structures and some surface functional groups on PBC500. For instance, the reaction between HSO_5^- and the electrons of C=O can result in the formation of $SO_4^{\cdot-}$ (Equation (4)) [73]. The generation of ·OH could be explained by the reactions of $SO_4^{\cdot-}$ and H_2O/OH^- (Equations (5) and (6)) [74]. In addition, the defect structures of biochar can also donate electrons to HSO_5^- for generating $SO_4^{\cdot-}$ and ·OH (Equations

(7) and (8)) [48]. It was possible that interactions between activated PMS can lead to the production of $^1O_2$ (Equations (9)–(11)) [75]. The $S_2O_8^{2-}$ can be adsorbed onto C=O to generate O_2^{-} (Equation (12)) [76]. Finally, the various ROS generated on the surface of PBC500 could be transported into solutions and degrade E2 through both radical and non-radical ways.

$$C{=}O + HSO_5^- \rightarrow SO_4^- + C\text{-}O^+ + OH^- \quad (4)$$

$$SO_4^- + H_2O \rightarrow SO_4^{2-} + \cdot OH + H^+ \quad (5)$$

$$SO_4^- + OH^- \rightarrow SO_4^{2-} + HSO_4^- + \cdot OH \quad (6)$$

$$HSO_5^- + BC_{defects} \rightarrow SO_4^- + OH^- + BC_{defects}^- \quad (7)$$

$$HSO_5^- + BC_{defects} \rightarrow \cdot OH + SO_4^{2-} + BC_{defects}^- \quad (8)$$

$$HSO_5^- + SO_4^- \rightarrow HSO_4^- + SO_5^- \quad (9)$$

$$SO_5^- + SO_5^- \rightarrow 2SO_4^- + {}^1O_2 \quad (10)$$

$$SO_5^- + SO_5^- \rightarrow S_2O_8^{2-} + {}^1O_2 \quad (11)$$

$$C{=}O + S_2O_8^{2-} \rightarrow C\text{-}O^+ + SO_4^{2-} + O_2^- \quad (12)$$

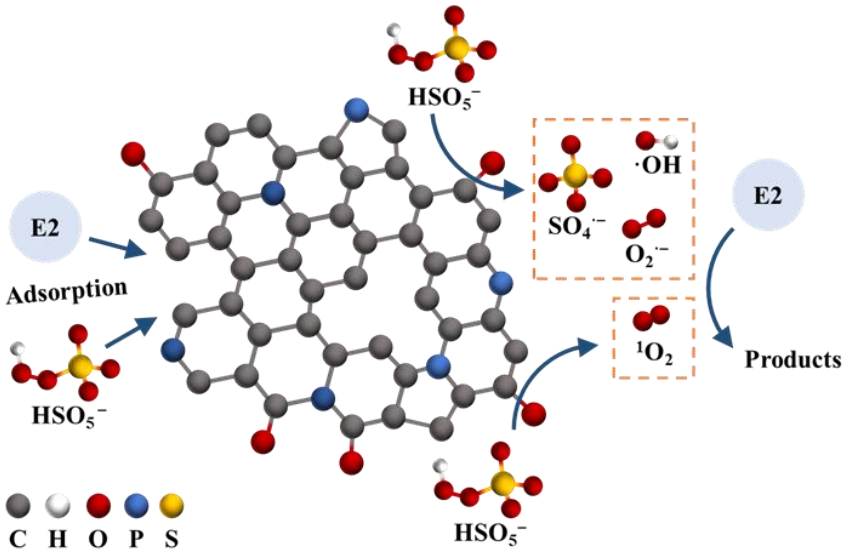

Figure 7. Mechanism of PMS activated by PBC500 for E2 degradation.

3.5. The Reuse of PBC500

3.5.1. The Reusability of PBC500

In order to assess the reusability of PBC500, the recycle experiments were carried out. The following can be seen from Figure 8a: the activation performance of PBC500 declined with a higher number of cycle times. The removal efficiencies of E2 within 90 min decreased from 97.91% to 88.07% and 65.15% after the second and third cycle times, respectively. The deactivation of PBC500 may be a consequence of the blockage of active sites induced by the accumulation of E2 and its degradation intermediates onto the surface of PBC500 [77].

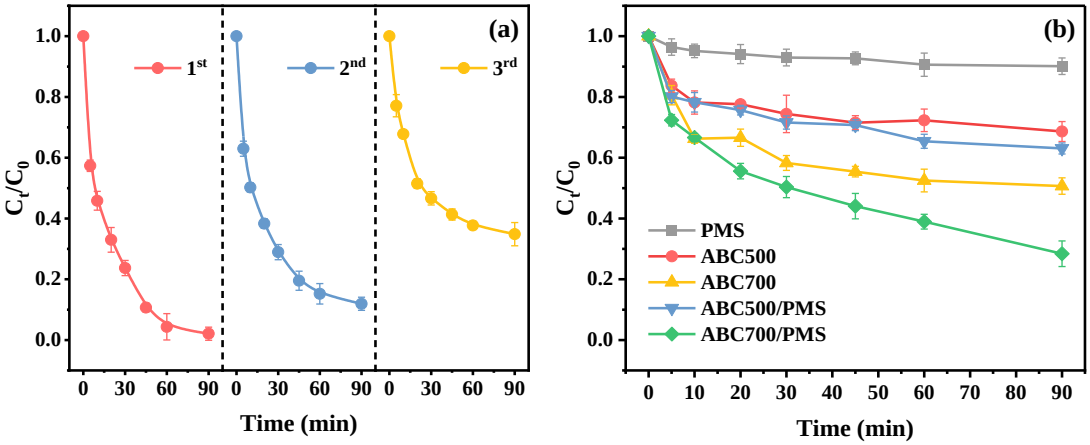

Figure 8. (**a**) The reusability of the PBC500/PMS system in three consecutive cycles and (**b**) the adsorption and catalytic performance of ash modified biochar (experiment conditions: [E2] = 3 mg/L, [PMS] = 1.0 mM, and [biochar] = 0.2 g/L).

3.5.2. The Ash of PBC500 Used as a Modifier

Figure 8b displays the adsorption and activation capacity of ash modified biochar prepared under various pyrolysis temperature conditions. In the case of PMS absence, the E2 removal by ABC500 relying on adsorption was only 31.31% within 90 min. Although the removal of E2 was improved to a certain extent by the ABC500/PMS system, it was only 36.95% after 90 min of reaction. It was apparent that ash modification treatment enhanced the removal by biochar under the conditions of adding or not adding PMS, but it was still weaker than that of the phosphoric acid modified biochar. This might be due to the limited phosphate content in the ash. The adsorption and catalytic performance of the ash modified biochar were remarkably improved by the rise in pyrolysis temperature. The removal efficiencies of E2 by ABC700 and the ABC700/PMS were 49.23% and 71.59%, respectively, which may account for the increase in specific surface area and reaction sites under higher pyrolysis temperature conditions [78]. Therefore, it could be concluded that the application of the ash from exhausted PBC500 as a modifier was an effective approach to improve the ability to adsorb and catalyze the original biochar.

4. Conclusions

To sum up, the modified biochar materials were successfully prepared by pyrolysis from cow manure that had been impregnated with phosphoric acid and applied as a catalyst to activate PMS for E2 degradation. In comparison with unmodified biochar, the phosphoric acid-treated biochar exhibited a significant increase in specific surface area, graphite degree, defective structures, and surface functional groups and showed excellent catalytic activity to activate PMS. The quenching experiments revealed that radical processes ($SO_4^{\cdot-}$, ·OH, and $O_2^{\cdot-}$) and non-radicals ($^1O_2$) contributed to the removal of E2, and $O_2^{\cdot-}$ and $^1O_2$ were the dominant reactive oxygen species for pollutant degradation. The abundant defective structures, carbonyl functional groups and P-containing functional groups on PBC500 can serve as effective active sites for reactive oxygen species formation. In addition, the reusability of PBC500 is relatively good, and the residual ash from the pyrolysis of exhausted PBC500 could be used as a modifier to enhance the adsorption and catalytic capacity of the original biochar. This work not only successfully achieved the conversion of livestock manure waste into resources but also provided a phosphoric acid modified biochar as an effective catalyst for PMS activation in the abatement of contaminations.

Supplementary Materials: The following supporting information can be downloaded at: https://www.mdpi.com/article/10.3390/w16121754/s1, Text S1. Kinetic modelling analysis. Text S2. Characterization methods. Text S3. analytic methods. Table S1 The total P content in CBC500 and PBC500. Table S2 Properties of pristine and P-doped biochar. Table S3 Element composition of

biochar. Table S4 High deconvolution of C1s XPS spectra of CBC500 and PBC500 before and after E2 degradation. Table S6 High deconvolution of P 2p XPS spectra of PBC500 before and after E2 degradation. Figure S1. The (a) adsorption and (b) catalytic performance of phosphoric acid modified biochar prepared at different pyrolysis temperatures (experiment conditions: [E2] = 3 mg/L, [PMS] = 2.0 mM, [biochar] = 0.1 g/L). Figure S2. The (a) adsorption and (b) catalytic performance of modified biochar impregnated with different concentrations of phosphoric acid. (experiment conditions: [E2] = 3 mg/L, [PMS] = 2.0 mM, [biochar] = 0.1 g/L). Figure S3. The adsorption and catalytic performance of CBC 500 and PBC500. (experiment conditions: [E2] = 3 mg/L, [PMS] = 2.0 mM, [biochar] = 0.1 g/L). Figure S4. Zeta potential of PBC500 at different pH values. Figure S5. Kinetic fitting curves of E2 degradation at different (a) PBC500 dosage, (b) PMS concentration, (c) E2 concentration, (d) pH, (e) Cl- concentration and (f) HA concentration. Figure S6. (a) C 1s, (b) O 1s and (c) P 2p XPS spectra of CBC500 after the reaction. References [79,80] are cited in the Supplementary Materials.

Author Contributions: W.Y.: Investigation, Data analysis, Validation, Writing—original draft, Writing—review and editing, Funding acquisition. G.F.: Investigation, Data analysis, Validation, Writing—original draft, Writing—review and editing, Funding acquisition. J.Z. (Junhou Zhou): Investigation, Data analysis, Validation, Writing—original draft. R.L.: Investigation, Data analysis, Validation. X.C.: Data analysis, Validation, Writing—review and editing. Y.S., J.L., J.Z. (Jianyong Zou), Z.H., K.-Q.X. and Q.L.: Validation, Writing—review and editing. All authors have read and agreed to the published version of the manuscript.

Funding: This research was funded by the Natural Science Foundation of Fujian Province in China (No. 2021N0022, 2021Y3002, 2023J02006), the Science and Technology Research Project of Housing and Urban-Rural Development in Fujian Province (No. 2022-K-2) and the Science and Technology Project of Anhui Province (No. 2021-YF26).

Data Availability Statement: Data are contained within the article and Supplementary Materials.

Acknowledgments: The authors would like to the Natural Science Foundation of Fujian Province in China (No. 2021N0022, 2021Y3002, 2023J02006), the Science and Technology Research Project of Housing and Urban-Rural Development in Fujian Province (No. 2022-K-2) and the Science and Technology Project of Anhui Province (No. 2021-YF26).

Conflicts of Interest: Author Jing Luo was employed by the company Fujian Jinhuang Environmental Sci-Tech Co., Ltd. Author Jianyong Zou was employed by the company Anhui Urban Construction Design Institute Co., Ltd. Author Zhanglin Hong was employed by the company China Construction Third Bureau First Engineering Co., Ltd. The remaining authors declare that the research was conducted in the absence of any commercial or financial relationships that could be construed as a potential conflict of interest.

References

1. Xu, H.H.; Han, Y.P.; Wang, G.Z.; Deng, P.Y.; Feng, L.L. Walnuat shell biochar based sorptive remediation of estrogens polluted simulated wastewater: Characterization, adsorption mechanism and degradation by persistent free radicals. *Environ. Technol. Innov.* **2022**, *28*, 102870. [CrossRef]
2. Peiris, C.; Nawalage, S.; Wewalwela, J.J.; Gunatilake, S.R.; Vithanage, M. Biochar based sorptive remediation of steroidal estrogen contaminated aqueous systems: A critical review. *Environ. Res.* **2020**, *191*, 110183. [CrossRef] [PubMed]
3. Zhang, P.; Liu, S.B.; Tan, X.F.; Liu, Y.G.; Zeng, G.M.; Yin, Z.H.; Ye, S.J.; Zeng, Z.W. Microwave-assisted chemical modification method for surface regulation of biochar and its application for estrogen removal. *Process Saf. Environ. Prot.* **2019**, *128*, 329–341. [CrossRef]
4. Sun, W.L.; Zhang, C.S.; Xu, N.; Ni, J.R. Effect of inorganic nanoparticles on 17 beta-estradiol and 17 alpha-ethynylestradiol adsorption by multi-walled carbon nanotubes. *Environ. Pollut.* **2015**, *205*, 111–120. [CrossRef] [PubMed]
5. Yin, Z.H.; Liu, Y.G.; Tan, X.F.; Jiang, L.H.; Zeng, G.M.; Liu, S.B.; Tian, S.R.; Liu, S.J.; Liu, N.; Li, M.F. Adsorption of 17 beta-estradiol by a novel attapulgite/biochar nanocomposite: Characteristics and influencing factors. *Process Saf. Environ. Prot.* **2019**, *121*, 155–164. [CrossRef]
6. Qing, Y.S.; Li, Y.X.; Guo, Z.W.; Yang, Y.J.; Li, W.L. Photocatalytic Bi_2WO_6/pg-C_3N_4-embedded in polyamide microfiltration membrane with enhanced performance in synergistic adsorption-photocatalysis of 17 beta-estradiol from water. *J. Environ. Chem. Eng.* **2022**, *10*, 108648. [CrossRef]
7. Oh, W.D.; Dong, Z.L.; Lim, T.T. Generation of sulfate radical through heterogeneous catalysis for organic contaminants removal: Current development, challenges and prospects. *Appl. Catal. B Environ.* **2016**, *194*, 169–201. [CrossRef]
8. Guo, S.; Chen, M.; Wei, Y.; You, L.; Cai, C.; Wei, Q.; Zhou, K. Designing hierarchically porous zero-valent iron via 3D printing to degrade organic pollutants by activating peroxymonosulfate using high-valent iron-oxo species. *Chem. Eng. J.* **2023**, *476*, 146523. [CrossRef]

9. Wang, J.L.; Wang, S.Z. Activation of persulfate (PS) and peroxymonosulfate (PMS) and application for the degradation of emerging contaminants. *Chem. Eng. J.* **2018**, *334*, 1502–1517. [CrossRef]
10. Peng, L.J.; Shang, Y.N.; Gao, B.Y.; Xu, X. Co_3O_4 anchored in N, S heteroatom co-doped porous carbons for degradation of organic contaminant: Role of pyridinic N-Co binding and high tolerance of chloride. *Appl. Catal. B Environ.* **2021**, *282*, 119484. [CrossRef]
11. Milh, H.; Cabooter, D.; Dewil, R. Role of process parameters in the degradation of sulfamethoxazole by heat-activated peroxymonosulfate oxidation: Radical identification and elucidation of the degradation mechanism. *Chem. Eng. J.* **2021**, *422*, 130457. [CrossRef]
12. Lee, Y.; Lee, S.; Cui, M.C.; Ren, Y.M.; Park, B.; Ma, J.J.; Han, Z.C.; Khim, J. Activation of peroxodisulfate and peroxymonosulfate by ultrasound with different frequencies: Impact on ibuprofen removal efficient, cost estimation and energy analysis. *Chem. Eng. J.* **2021**, *413*, 127487. [CrossRef]
13. Luo, C.W.; Gao, J.; Ma, Q.; Wu, D.J.; Cheng, X.X.; Jiang, J.; Zhou, W.W.; Yang, Z.C.; Ma, J. The bromate formation accompanied by the degradation of 2,4-bromophenol in UV/peroxymonosulfate. *Sep. Purif. Technol.* **2020**, *233*, 116028. [CrossRef]
14. Wang, J.Q.; Hasaer, B.; Yang, M.; Liu, R.P.; Hu, C.Z.; Liu, H.J.; Qu, J.H. Anaerobically-digested sludge disintegration by transition metal ions-activated peroxymonosulfate (PMS): Comparison between Co^{2+}, Cu^{2+}, Fe^{2+} and Mn^{2+}. *Sci. Total Environ.* **2020**, *713*, 136530. [CrossRef] [PubMed]
15. Li, W.; Wu, P.X.; Zhu, Y.J.; Huang, Z.J.; Lu, Y.H.; Li, Y.W.; Dang, Z.; Zhu, N.W. Catalytic degradation of bisphenol A by CoMnAl mixed metal oxides catalyzed peroxymonosulfate: Performance and mechanism. *Chem. Eng. J.* **2015**, *279*, 93–102. [CrossRef]
16. Solis, R.R.; Mena, I.F.; Nadagouda, M.N.; Dionysiou, D.D. Adsorptive interaction of peroxymonosulfate with graphene and catalytic assessment via non-radical pathway for the removal of aqueous pharmaceuticals. *J. Hazard. Mater.* **2020**, *384*, 121340. [CrossRef] [PubMed]
17. Chen, J.B.; Zhang, L.M.; Huang, T.Y.; Li, W.W.; Wang, Y.; Wang, Z.M. Decolorization of azo dye by peroxymonosulfate activated by carbon nanotube: Radical versus non-radical mechanism. *J. Hazard. Mater.* **2016**, *320*, 571–580. [CrossRef] [PubMed]
18. Yun, E.T.; Moon, G.H.; Lee, H.; Jeon, T.H.; Lee, C.; Choi, W.; Lee, J. Oxidation of organic pollutants by peroxymonosulfate activated with low-temperature-modified nanodiamonds: Understanding the reaction kinetics and mechanism. *Appl. Catal. B Environ.* **2018**, *237*, 432–441. [CrossRef]
19. Ouyang, D.; Chen, Y.; Chen, R.H.; Zhang, W.Y.; Yan, J.C.; Gu, M.Y.; Li, J.; Zhang, H.B.; Chen, M.F. Degradation of 1,4-dioxane by biochar activating peroxymonosulfate under continuous flow conditions. *Sci. Total Environ.* **2022**, *809*, 151929. [CrossRef]
20. Liang, L.P.; Xi, F.F.; Tan, W.S.; Meng, X.; Hu, B.W.; Wang, X.K. Review of organic and inorganic pollutants removal by biochar and biochar-based composites. *Biochar* **2021**, *3*, 255–281. [CrossRef]
21. Xie, M.X.; Chen, W.; Xu, Z.Y.; Zheng, S.R.; Zhu, D.Q. Adsorption of sulfonamides to demineralized pine wood biochars prepared under different thermochemical conditions. *Environ. Pollut.* **2014**, *186*, 187–194. [CrossRef]
22. Mushtaq, M.; Zeshan, M.; Zeeshan, M.; Nawaz, I.; Hassan, M. Effect of low levels of oxytetracycline on anaerobic digestion of cattle manure. *Bioresour. Technol.* **2022**, *349*, 126894. [CrossRef]
23. Zhang, H.; Shi, J.H.; Liu, X.W.; Zhan, X.M.; Chen, Q.C. Occurrence and removal of free estrogens, conjugated estrogens, and bisphenol A in manure treatment facilities in East China. *Water Res.* **2014**, *58*, 248–257. [CrossRef]
24. Zhu, Y.; Yi, B.J.; Yuan, Q.X.; Wu, Y.L.; Wang, M.; Yan, S.P. Removal of methylene blue from aqueous solution by cattle manure-derived low temperature biochar. *RSC. Adv.* **2018**, *8*, 19917–19929. [CrossRef]
25. Tian, R.Q.; Li, C.X.; Xie, S.Y.; You, F.T.; Cao, Z.H.; Xu, Z.H.; Yu, G.W.; Wang, Y. Preparation of biochar via pyrolysis at laboratory and pilot scales to remove antibiotics and immobilize heavy metals in livestock feces. *J. Soils Sediments* **2019**, *19*, 2891–2902. [CrossRef]
26. Hoffman, T.C.; Zitomer, D.H.; McNamara, P.J. Pyrolysis of wastewater biosolids significantly reduces estrogenicity. *J. Hazard. Mater.* **2016**, *317*, 579–584. [CrossRef]
27. Xi, J.; Wang, Q.; Liu, J.; Huan, L.; He, Z.; Qiu, Y.; Zhang, J.; Tang, C.; Xiao, J.; Wang, S. N,P-dual-doped multilayer graphene as an efficient carbocatalyst for nitroarene reduction: A mechanistic study of metal-free catalysis. *J. Catal.* **2018**, *359*, 233–241. [CrossRef]
28. Liang, X.; Zhao, Y.; Liu, J.; Yang, Z.; Yang, Q. Highly efficient activation of peroxymonosulfate by cobalt ferrite anchored in P-doped activated carbon for degradation of 2,4-D: Adsorption and electron transfer mechanism. *J. Colloid Interface Sci.* **2023**, *642*, 757–770. [CrossRef]
29. Huang, P.; Zhang, P.; Wang, C.P.; Du, X.; Jia, H.Z.; Sun, H.W. P-doped biochar regulates nZVI nanocracks formation for superefficient persulfate activation. *J. Hazard. Mater.* **2023**, *450*, 130999. [CrossRef]
30. Yu, J.F.; Tang, L.; Pang, Y.; Zhou, Y.Y.; Feng, H.P.; Ren, X.Y.; Tang, J.; Wang, J.J.; Deng, L.F.; Shao, B.B. Non-radical oxidation by N,S,P co-doped biochar for persulfate activation: Different roles of exogenous P/S doping, and electron transfer path. *J. Clean. Prod.* **2022**, *374*, 133995. [CrossRef]
31. Zeng, X.Y.; Wang, Y.; Li, R.X.; Cao, H.L.; Li, Y.F.; Lu, J. Impacts of temperatures and phosphoric-acid modification to the physicochemical properties of biochar for excellent sulfadiazine adsorption. *Biochar* **2022**, *4*, 14. [CrossRef]
32. Zhao, S.; Zhang, L.J.; Hu, H.Q.; Jin, L.J. Catalytic decomposition of methane over enteromorpha prolifera-based hierarchical porous biochar. *Int. J. Hydrogen Energy* **2023**, *48*, 3328–3339. [CrossRef]
33. Zhou, M.L.; Xu, Y.; Luo, G.Q.; Zhang, Q.Z.; Du, L.; Cui, X.W.; Li, Z.H. Facile synthesis of phosphorus-doped porous biochars for efficient removal of elemental mercury from coal combustion flue gas. *Chem. Eng. J.* **2022**, *432*, 134440. [CrossRef]

34. Yadav, K.; Tyagi, M.; Kumari, S.; Jagadevan, S. Influence of Process Parameters on Optimization of Biochar Fuel Characteristics Derived from Rice Husk: A Promising Alternative Solid Fuel. *Bioenergy Res.* **2019**, *12*, 1052–1065. [CrossRef]
35. Tsai, W.T.; Huang, C.N.; Chen, H.R.; Cheng, H.Y. Pyrolytic Conversion of Horse Manure into Biochar and Its Thermochemical and Physical Properties. *Waste Biomass Valorization* **2015**, *6*, 975–981. [CrossRef]
36. Danish, M.; Ahmad, T. A review on utilization of wood biomass as a sustainable precursor for activated carbon production and application. *Renew. Sustain. Energy Rev.* **2018**, *87*, 1–21. [CrossRef]
37. Sing, K.S.W. Reporting physisorption data for gas/solid systems with special reference to the determination of surface area and porosity (Recommendations 1984). *Pure. Appl. Chem.* **1985**, *57*, 603–619. [CrossRef]
38. Li, Y.; Ma, S.; Xu, S.; Fu, H.; Li, Z.; Li, K.; Sheng, K.; Du, J.; Lu, X.; Li, X.; et al. Novel magnetic biochar as an activator for peroxymonosulfate to degrade bisphenol A: Emphasizing the synergistic effect between graphitized structure and $CoFe_2O_4$. *Chem. Eng. J.* **2020**, *387*, 124094. [CrossRef]
39. Li, M.; Tang, Y.; Ren, N.; Zhang, Z.; Cao, Y. Effect of mineral constituents on temperature-dependent structural characterization of carbon fractions in sewage sludge-derived biochar. *J. Clean. Prod.* **2018**, *172*, 3342–3350. [CrossRef]
40. Zhang, P.Z.; Li, Y.F.; Cao, Y.Y.; Han, L.J. Characteristics of tetracycline adsorption by cow manure biochar prepared at different pyrolysis temperatures. *Bioresour. Technol.* **2019**, *285*, 121348. [CrossRef] [PubMed]
41. Feng, Z.Q.; Zhou, B.H.; Yuan, R.F.; Li, H.Q.; He, P.D.; Wang, F.; Chen, Z.B.; Chen, H.L. Biochar derived from different crop straws as persulfate activator for the degradation of sulfadiazine: Influence of biomass types and systemic cause analysis. *Chem. Eng. J.* **2022**, *440*, 135669. [CrossRef]
42. Ma, F.W.; Ma, D.; Wu, G.; Geng, W.D.; Shao, J.Q.; Song, S.J.; Wan, J.F.; Qiu, J.S. Construction of 3D nanostructure hierarchical porous graphitic carbons by charge-induced self-assembly and nanocrystal-assisted catalytic graphitization for supercapacitors. *Chem. Commun.* **2016**, *52*, 6673–6676. [CrossRef]
43. Zhang, W.; Yan, L.; Wang, Q.; Li, X.; Guo, Y.; Song, W.; Li, Y. Ball milling boosted the activation of peroxymonosulfate by biochar for tetracycline removal. *J. Environ. Chem. Eng.* **2021**, *9*, 106870. [CrossRef]
44. Wang, P.; Cao, J.; Mao, L.; Zhu, L.; Zhang, Y.; Zhang, L.; Jiang, H.; Zheng, Y.; Liu, X. Effect of H_3PO_4-modified biochar on the fate of atrazine and remediation of bacterial community in atrazine-contaminated soil. *Sci. Total Environ.* **2022**, *851*, 158278. [CrossRef]
45. Guo, J.; Zheng, L.; Li, Z.; Zhou, X.; Cheng, S.; Zhang, L. Effects of various pyrolysis conditions and feedstock compositions on the physicochemical characteristics of cow manure-derived biochar. *J. Clean. Prod.* **2021**, *311*, 127458. [CrossRef]
46. Xie, X.; Shi, J.; Pu, Y.; Wang, Z.Y.; Zhang, L.L.; Wang, J.X.; Wang, D. Cellulose derived nitrogen and phosphorus co-doped carbon-based catalysts for catalytic reduction of p-nitrophenol. *J. Colloid. Interface. Sci.* **2020**, *571*, 100–108. [CrossRef]
47. Shi, C.F.; Hu, K.; Nie, L.Y.; Wang, H.R.; Ma, L.L.; Du, Q.; Wang, G.X. Degradation of acetaminophen using persulfate activated with P-doped biochar and thiosulfate. *Inorg. Chem. Commun.* **2022**, *146*, 110160. [CrossRef]
48. Ouyang, D.; Chen, Y.; Yan, J.C.; Qian, L.B.; Han, L.; Chen, M.F. Activation mechanism of peroxymonosulfate by biochar for catalytic degradation of 1,4-dioxane: Important role of biochar defect structures. *Chem. Eng. J.* **2019**, *370*, 614–624. [CrossRef]
49. Lyu, H.; Gao, B.; He, F.; Ding, C.; Tang, J.; Crittenden, J.C. Ball-Milled Carbon Nanomaterials for Energy and Environmental Applications. *ACS Sustain. Chem. Eng.* **2017**, *5*, 9568–9585. [CrossRef]
50. Qian, Y.; Jiang, S.; Li, Y.; Yi, Z.; Zhou, J.; Li, T.Q.; Han, Y.; Wang, Y.S.; Tian, J.; Lin, N.; et al. In Situ Revealing the Electroactivity of P-O and P-C Bonds in Hard Carbon for High-Capacity and Long-Life Li/K-Ion Batteries. *Adv. Energy Mater.* **2019**, *9*, 1901676. [CrossRef]
51. Tomczyk, A.; Sokolowska, Z.; Boguta, P. Biochar physicochemical properties: Pyrolysis temperature and feedstock kind effects. *Rev. Environ. Sci. Biotechnol.* **2020**, *19*, 191–215. [CrossRef]
52. Jagtoyen, M.; Derbyshire, F. Activated carbons from yellow poplar and white oak by H_3PO_4 activation. *Carbon* **1998**, *36*, 1085–1097. [CrossRef]
53. Ounas, A.; Aboulkas, A.; El Harfi, K.; Bacaoui, A.; Yaacoubi, A. Pyrolysis of olive residue and sugar cane bagasse: Non-isothermal thermogravimetric kinetic analysis. *Bioresour. Technol.* **2011**, *102*, 11234–11238. [CrossRef]
54. Zhang, D.H.; Lin, X.N.; Zhang, Q.F.; Ren, X.J.; Yu, W.F.; Cai, H.Z. Catalytic pyrolysis of wood-plastic composite waste over activated carbon catalyst for aromatics production: Effect of preparation process of activated carbon. *Energy* **2020**, *212*, 118983. [CrossRef]
55. Ma, Y.F.; Tang, J.Y.; Chen, S.Y.; Yang, L.; Shen, S.T.; Chen, X.; Zhang, Z.L. Ball milling and acetic acid co-modified sludge biochar enhanced by electrochemistry to activate peroxymonosulfate for sustainable degradation of environmental concentration neonicotinoids. *J. Hazard. Mater.* **2023**, *444*, 130336. [CrossRef]
56. Zhang, P.; Tan, X.; Liu, S.; Liu, Y.; Zeng, G.; Ye, S.; Yin, Z.; Hu, X.; Liu, N. Catalytic degradation of estrogen by persulfate activated with iron-doped graphitic biochar: Process variables effects and matrix effects. *Chem. Eng. J.* **2019**, *378*, 122141. [CrossRef]
57. Zhang, Z.L.; Ding, H.; Li, Y.; Yu, J.; Ding, L.; Kong, Y.L.; Ma, J.Y. Nitrogen-doped biochar encapsulated Fe/Mn nanoparticles as cost-effective catalysts for heterogeneous activation of peroxymonosulfate towards the degradation of bisphenol-A: Mechanism insight and performance assessment. *Sep. Purif. Technol.* **2022**, *283*, 120136. [CrossRef]
58. Ren, W.B.; Huang, X.K.; Wang, L.X.; Liu, X.T.; Zhou, Z.; Wang, Y.Q.; Lin, C.Y.; He, M.C.; Ouyang, W. Degradation of simazine by heat-activated peroxydisulfate process: A coherent study on kinetics, radicals and models. *Chem. Eng. J.* **2021**, *426*, 131876. [CrossRef]

59. Huong, P.T.; Jitae, K.; Al Tahtamouni, T.M.; Tri, N.L.M.; Kim, H.H.; Cho, K.H.; Lee, C. Novel activation of peroxymonosulfate by biochar derived from rice husk toward oxidation of organic contaminants in wastewater. *J. Water Process Eng.* **2020**, *33*, 101037. [CrossRef]
60. Ren, Y.M.; Lin, L.Q.; Ma, J.; Yang, J.; Feng, J.; Fan, Z.J. Sulfate radicals induced from peroxymonosulfate by magnetic ferrospinel MFe_2O_4 (M = Co, Cu, Mn, and Zn) as heterogeneous catalysts in the water. *Appl. Catal. B Environ.* **2015**, *165*, 572–578. [CrossRef]
61. Ahmadi, M.; Ghanbari, F. Organic dye degradation through peroxymonosulfate catalyzed by reusable graphite felt/ferriferrous oxide: Mechanism and identification of intermediates. *Mater. Res. Bull.* **2019**, *111*, 43–52. [CrossRef]
62. Bai, L.M.; Liu, Z.H.; Wang, H.R.; Li, G.B.; Liang, H. Fe(II)-activated peroxymonosulfate coupled with nanofiltration removes natural organic matter and sulfamethoxazole in natural surface water: Performance and mechanisms. *Sep. Purif. Technol.* **2021**, *274*, 119088. [CrossRef]
63. Lee, Y.; Yoon, J.; Von Gunten, U. Kinetics of the oxidation of phenols and phenolic endocrine disruptors during water treatment with ferrate (Fe(VI)). *Environ. Sci. Technol.* **2005**, *39*, 8978–8984. [CrossRef]
64. Fu, H.C.; Zhao, P.; Xu, S.J.; Cheng, G.; Li, Z.Q.; Li, Y.; Li, K.; Ma, S.L. Fabrication of Fe_3O_4 and graphitized porous biochar composites for activating peroxymonosulfate to degrade p-hydroxybenzoic acid: Insights on the mechanism. *Chem. Eng. J.* **2019**, *375*, 121980. [CrossRef]
65. Zhu, K.; Bin, Q.; Shen, Y.Q.; Huang, J.; He, D.D.; Chen, W.J. In-situ formed N-doped bamboo-like carbon nanotubes encapsulated with Fe nanoparticles supported by biochar as highly efficient catalyst for activation of persulfate (PS) toward degradation of organic pollutants. *Chem. Eng. J.* **2020**, *402*, 126090. [CrossRef]
66. Lau, A.Y.T.; Tsang, D.C.W.; Graham, N.J.D.; Ok, Y.S.; Yang, X.; Li, X.D. Surface-modified biochar in a bioretention system for Escherichia coli removal from stormwater. *Chemosphere* **2017**, *169*, 89–98. [CrossRef]
67. Outsiou, A.; Frontistis, Z.; Ribeiro, R.S.; Antonopoulou, M.; Konstantinou, I.K.; Silva, A.M.T.; Faria, J.L.; Gomes, H.T.; Mantzavinos, D. Activation of sodium persulfate by magnetic carbon xerogels (CX/CoFe) for the oxidation of bisphenol A: Process variables effects, matrix effects and reaction pathways. *Water Res.* **2017**, *124*, 97–107. [CrossRef]
68. Fan, J.H.; Qin, H.H.; Jiang, S.M. Mn-doped g-C_3N_4 composite to activate peroxymonosulfate for acetaminophen degradation: The role of superoxide anion and singlet oxygen. *Chem. Eng. J.* **2019**, *359*, 723–732. [CrossRef]
69. Chen, X.; Qian, S.F.; Ma, Y.F.; Zhu, J.Y.; Shen, S.T.; Ding, Y.Z.; Zhi, S.L.; Zhang, K.Q.; Yang, L.; Zhang, Z.L. Efficient degradation of sulfamethoxazole in various waters with peroxymonosulfate activated by magnetic-modified sludge biochar: Surface-bound radical mechanism. *Environ. Pollut.* **2023**, *319*, 121010. [CrossRef]
70. Liu, J.J.; Zou, S.H.; Xiao, L.P.; Fan, J. Well-dispersed bimetallic nanoparticles confined in mesoporous metal oxides and their optimized catalytic activity for nitrobenzene hydrogenation. *Catal. Sci. Technol.* **2014**, *4*, 441–446. [CrossRef]
71. Zhang, X.B.; Yang, Y.Y.; Ngo, H.H.; Guo, W.S.; Sun, F.X.; Wang, X.; Zhang, J.Q.; Long, T.W. Urea removal in reclaimed water used for ultrapure water production by spent coffee biochar/granular activated carbon activating peroxymonosulfate and peroxydisulfate. *Bioresour. Technol.* **2022**, *343*, 126062. [CrossRef] [PubMed]
72. Hua, L.; Cheng, T.Z.; Liang, Z.Y.; Wei, T. Investigation of the mechanism of phytate-modified biochar-catalyzed persulfate degradation of Ponceau 2R. *Biochar* **2022**, *4*, 6. [CrossRef]
73. Li, J.Q.; Li, M.T.; Sun, H.Q.; Ao, Z.M.; Wang, S.B.; Liu, S.M. Understanding of the Oxidation Behavior of Benzyl Alcohol by Peroxymonosulfate via Carbon Nanotubes Activation. *ACS Catal.* **2020**, *10*, 3516–3525. [CrossRef]
74. Duan, X.G.; Su, C.; Zhou, L.; Sun, H.Q.; Suvorova, A.; Odedairo, T.; Zhu, Z.H.; Shao, Z.P.; Wang, S.B. Surface controlled generation of reactive radicals from persulfate by carbocatalysis on nanodiamonds. *Appl. Catal. B Environ.* **2016**, *194*, 7–15. [CrossRef]
75. Guo, Y.; Yan, L.; Li, X.; Yan, T.; Song, W.; Hou, T.; Tong, C.; Mu, J.; Xu, M. Goethite/biochar-activated peroxymonosulfate enhances tetracycline degradation: Inherent roles of radical and non-radical processes. *Sci. Total Environ.* **2021**, *783*, 147102. [CrossRef] [PubMed]
76. Yang, H.; Qiu, R.; Tang, Y.; Ye, S.; Wu, S.; Qin, F.; Xiang, L.; Tan, X.; Zeng, G.; Yan, M. Carbonyl and defect of metal-free char trigger electron transfer and $O_2^{\cdot-}$ in persulfate activation for Aniline aerofloat degradation. *Water Res.* **2023**, *231*, 119659. [CrossRef] [PubMed]
77. Tian, W.J.; Lin, J.K.; Zhang, H.Y.; Duan, X.G.; Wang, H.; Sun, H.Q.; Wang, S.B. Kinetics and mechanism of synergistic adsorption and persulfate activation by N-doped porous carbon for antibiotics removals in single and binary solutions. *J. Hazard. Mater.* **2022**, *423*, 127083. [CrossRef] [PubMed]
78. Chen, K.; Ma, D.; Yu, H.; Zhang, S.; Seyler, B.C.; Chai, Z.; Peng, S. Biosorption of V(V) onto Lantana camara biochar modified by H_3PO_4: Characteristics, mechanism, and regenerative capacity. *Chemosphere* **2022**, *291*, 132721. [CrossRef]
79. Xu, G.; Zhang, Y.; Shao, H.B.; Sun, J.N. Pyrolysis temperature affects phosphorus transformation in biochar: Chemical fractionation and 31P NMR analysis. *Sci. Total Environ.* **2016**, *569*, 65–72. [CrossRef]
80. Murphy, J.; Riley, J.P. Citation-Classic—A modified single solution method for the determination of phosphate in natural-waters. In *Current Contents/Agriculture Biology & Environmental Sciences*; Clarivate Analytics: Singapore, 1986; p. 16.